catalysts

MDPI

Article

Shapes Control of Bi_2WO_6 Nano-Structures as Photo-Fenton Catalysts for Pulping Wastewater Treatment

Miao Ran [1,2,†], Xiuxiu Zou [1,†], Qingwen Tian [1], Long Liang [1], Ting Wu [1], Aixiang Pan [1], Yongjun Deng [1], Guigan Fang [1,*] and Laibao Ding [1,*]

1 Institute of Chemical Industry of Forest Products, Chinese Academy of Forestry, Key Lab of Biomass Engineering and Material Jiangsu Province, National Engineering Lab for Biomass Chemical Utilization, Key and Open Lab of Forest Chemical Engineering, SAF, Nanjing 210042, China; ranmiaolhs@163.com (M.R.); zouxiuxiuxiu@163.com (X.Z.); tianqingwen@icifp.cn (Q.T.); lianglong@icifp.cn (L.L.); wuting@icifp.cn (T.W.); pax@icifp.cn (A.P.); dengyongjun@icifp.cn (Y.D.)

2 College of Light Industry Science and Engineering, Nanjing Forestry University, Nanjing 210037, China

* Correspondence: ppfangguigan@163.com (G.F.); dingyua2019@163.com (L.D.); Tel.: +86-025-854-82542 (L.D.); Fax: +86-025-854-13445 (L.D.)

† These authors contributed equally to this work.

Received: 20 November 2019; Accepted: 11 December 2019; Published: 14 December 2019

Abstract: Bi_2WO_6 assembled by flower-like microspheres and nanosheets were controllably synthesized through a one-step hydrothermal approach. Multiple technologies, including X-ray powder diffraction (XRD), scanning electron microscopy (SEM), and UV–Vis diffuse reflectance spectrum (UV–Vis), were carried out to characterize the as-synthesized samples. The photocatalytic efficiency of Bi_2WO_6 synthesized with a series of temperature and pH values shows different morphologies and photocatalytic properties. The photocatalyst (Bi_2WO_6) synthesized at 220 °C and pH of 7 exhibited the best photocatalytic performance, with the methylene blue (MB) degradation approaching 91.6% after reaction time of 60 min. Free radical capture experiments indicate that •OH is the primary reactive species in the methylene blue (MB) degradation reaction, h^+ and $\bullet O_2^-$ contribute negligible influence, while the addition of H_2O_2 significantly improves the photocatalytic activity of Bi_2WO_6. Biodegraded poplar preconditioning refiner chemical alkaline peroxide mechanical pulp wastewater (PPW) was treated over Bi_2WO_6 under UV light (Bi_2WO_6/UV/H_2O_2); chemical oxygen demand (COD_{Cr}) and color degradation rate were 85.8% and 92.0%, respectively. These results show that Bi_2WO_6 semiconductors can be introduced as an efficient and stable photocatalyst for industry wastewater treatment.

Keywords: Bi_2WO_6; photocatalytic activities; photo-Fenton-like reaction; pulping wastewater treatment

1. Introduction

In recent years, the pulp and paper industry has experienced rapid development, and its economic benefits have contributed to it becoming one of the most paramount industrial components in the world [1,2]. However, pulp and paper mills produce a massive amount of wastewater, which bring serious threats to the environment [3,4]. The as-obtained effluents derived from raw materials and production processes inevitably have a high chemical oxygen demand (COD) and low biodegradability properties, which usually consists of >200 organic compounds and total organic and inorganic species of approximately 700 [5,6]. Among those pollutants, dioxins, chlorate, chlorinated hydrocarbons, chloroform, phenols, and furans were observed, which are seriously harmful to human [7,8]. Pulp wastewater is usually treated by three processes, primary physicochemical

treatment, secondary biochemical treatment, and tertiary advanced treatment [9–11]. The primary physicochemical strategy was employed for removing colloidal particles, suspended solids, floating matters, toxic compounds, and colors from wastewaters [12,13]. The main steps include screening, sedimentation, flotation, flocculation, and coagulation [14]. Secondary biochemical treatment is the combination of anaerobic and aerobic treatment processes, which is efficient and economical for the treatment of soluble biodegradable organic components [15]. After two-stage processing, toxicity in the discharged effluents could be remarkably eliminated [16,17]. However, the effluents still contain parts of toxic organics, high color, and (suspended solids) SS, which need further treatment [4,6,18]. Coagulation and Fenton techniques were considered as the efficient and advanced treatment approaches, which have been applied in the wastewater treatment field [19]. During the reported processes, large amounts of sludge, high cost, and corrosion were generated, resulting in secondary pollution [20]. Therefore, developing an environmentally friendly and cost-efficient technique to deal with industrial wastewater is highly desirable, yet a challenge.

Photocatalytic degradation of organic pollutants over semiconductor catalysts have been studied and are regarded as an efficient means for environmental purification [21]. As a typical Aurivillius oxide photocatalyst, Bi_2WO_6 has been widely applied for mineralization of organic pollutants with UV light irradiation [22–24]. Thanks to its layered structure, Bi_2WO_6 possesses outstanding intrinsic physical and chemical properties [25–28]. Up to date, the facile hydrothermal route is still the dominant method for the preparation of Bi_2WO_6 photocatalyst, which affords a high crystallinity and size-controllable particles under mild conditions [27,29–31]. Herein, two kinds of bismuth tungsten oxides, including Bi_2WO_6 and $Bi_{14}W_2O_{27}$, were synthesized in this work under different pH and temperature conditions, and evaluated for the pulping wastewater treatment. The influences of pH and temperatures on the morphology transformation, photocatalysts activities of Bi_2WO_6, and its catalytic performance were then discussed systematically.

2. Results and Discussion

The crystalline structure of the synthesized samples were characterized by X-ray diffraction (XRD) technique. Figures 1 and 2 show the XRD patterns of temperature series samples corresponding with different pH values.

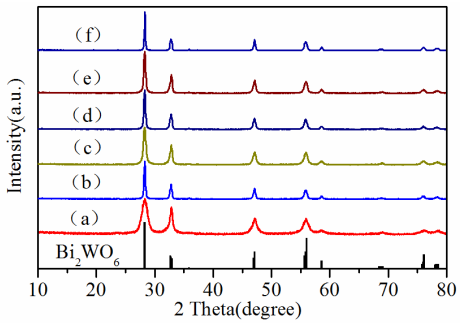

Figure 1. XRD patterns of prepared Bi_2WO_6 samples under different temperature and pH. (a) 140 °C, pH = 1; (b) 140 °C, pH = 7; (c) 180 °C, pH = 1; (d) 180 °C, pH = 7; (e) 220 °C, pH = 1; (f) 220 °C, pH = 7.

It is worth noting that different pH values produced different crystallized products, such as Bi_2WO_6 (pH = 1 or 7) and $Bi_{14}W_2O_{27}$ (pH = 13), as seen in Figures 1 and 2. The samples synthesized under the pH of 1 and 7 were well consistent with the standard card of orthorhombic Bi_2WO_6 according to the database of JCPDS NO.39-0256 [28]. The highest intensity peak at 28.54° belongs to (131) of Bi_2WO_6, the peaks positioned at 33.10°, 47.38°, 56.19°, and 58.69° in six patterns belong to (200), (202), (331), and (262) of the samples, respectively. However, the diffraction peaks from the samples obtained with pH of 13 were in good consistency with the standard card of orthorhombic $Bi_{14}W_2O_{27}$ according to the data base of JCPDS NO.39-0061 [29,32]. The diffraction peaks of the obtained samples were

determined at 2θ = 27.56°, 31.80°, 45.78°, 54.17°, 54.3°, indexing to the (312), (004), (424), (315), and (552) crystallographic planes of $Bi_{14}W_2O_{27}$, respectively. In addition, the crystallinity of Bi_2WO_6 can be greatly adjusted by pH values, especially at 140 °C, where an obvious higher crystallinity can be obtained at pH = 7 compared to pH = 1. The obtained sharp diffraction peaks demonstrate high crystallinity of the as-prepared sample powders.

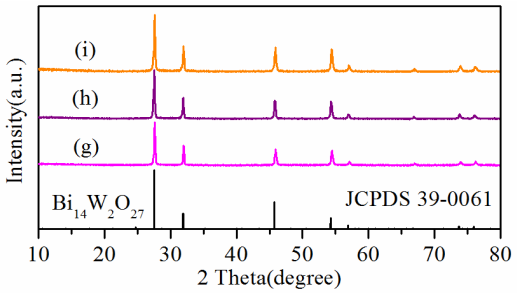

Figure 2. XRD patterns of prepared $Bi_{14}W_2O_{27}$ samples under different temperature and pH. (g) 140 °C, pH = 13; (h) 180 °C, pH = 13; (i) 220 °C, pH = 13.

For comparing the morphology and surface area of as-synthesized samples under different temperature and pH values, scanning electron microscopy (SEM) and BET were performed and are shown in Figure 3 and Table 1. It can be seen from Figure 3, the morphologies of products were significantly influenced by the pH value. The Bi_2WO_6 powders synthesized hydrothermally at pH of 1 exhibits 3D flower-like microspheres, which consist of the irregular nanosheets (Figure 3a,d,g). As the pH is increased up to 7, the morphology of Bi_2WO_6 consists of a large quantity of nanosheets (Figure 3b,e,h). In addition, both the morphology and composition of the obtained samples changed simultaneously as the pH value further increased to 13. $Bi_{14}W_2O_{27}$ was formed instead of Bi_2WO_6 and irregular granular particles are formed at the cost of the 3D flower-like microspheres and nanosheets. As seen in Table 1, the BET surface areas were significantly influenced by both pH and temperature. BET surface of Bi_2WO_6 was higher than $Bi_{14}W_2O_{27}$; Bi_2WO_6 was synthesized at 220 °C and pH of 1 (Table 1h) with the highest surface area 25.89 m^2/g.

Table 1. The surface area of Bi_2WO_6 and $Bi_{14}W_2O_{27}$.

	Sample	BET Area (m^2/g)
a	Bi_2WO_6-140 °C, pH = 1	9.73
b	Bi_2WO_6-140 °C, pH = 7	18.36
c	$Bi1_4W_2O_{27}$-140 °C, pH = 13	5.12
d	Bi_2WO_6-180 °C, pH = 1	11.88
e	Bi_2WO_6-180 °C, pH = 7	22.51
f	$Bi1_4W_2O_{27}$-180 °C, pH = 13	6.08
g	Bi_2WO_6-220 °C, pH = 1	14.67
h	Bi_2WO_6-220 °C, pH = 7	25.51
i	$Bi1_4W_2O_{27}$-220 °C, pH = 13	5.89

Figures 4 and 5 show the UV–Vis diffused reflectance spectra of the as-synthesized samples under different temperature and pH values. As observed in Figure 4, Bi_2WO_6 displays the photo-absorption property limited to 460 nm. The band gaps of the samples were calculated based on the formula below:

$$\alpha h\nu = A(h\upsilon - E_g)^{n/2},$$

where α, h, ν, A, E_g, and n are the absorption coefficient, Planck constant, light frequency, gap band energy, and a constant, respectively. Based on this equation, the value of n for both Bi_2WO_6 and $Bi_{14}W_2O_{27}$ was 1. A plot of $(\alpha h\nu)^2$ ~$h\nu$ according to the straight forward transition is shown as inset of

Figures 4 and 5, which were summarized in Table 2. The result shows that the band gaps of a, b, c, d, e, f were different, the values were 2.85, 2.80, 2.81, 2.79, 2.83, and 2.73 eV, respectively. As observed in Table 2, the band gaps of g, h, and i were 2.47, 2.43, and 2.41 eV, respectively. In general, Bi_2WO_6 has a better light absorption strength when the synthesized pH value is 7 and a high synthesis temperature can reduce the band gap of the catalysts.

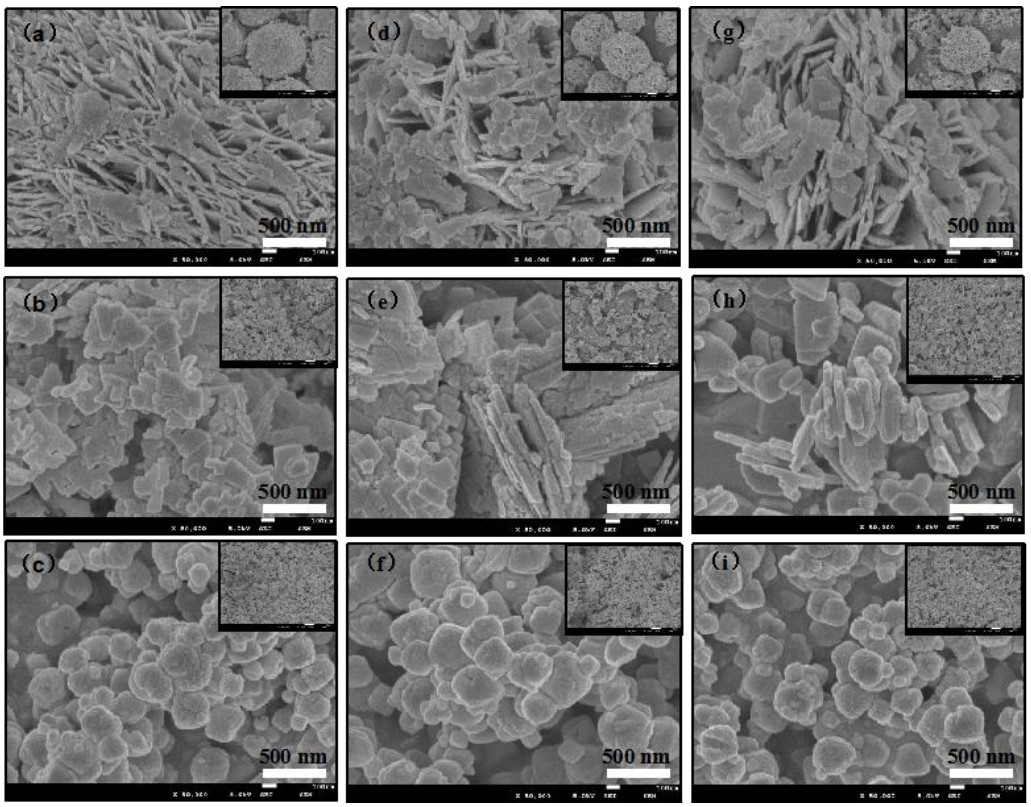

Figure 3. SEM images of prepared samples under different temperature and pH values. (**a**) 140 °C, pH = 1; (**b**) 140 °C, pH = 7; (**c**) 140 °C, pH = 13; (**d**) 180 °C, pH = 1; (**e**) 180 °C, pH = 7; (**f**) 180 °C, pH = 13; (**g**) 220 °C, pH = 1; (**h**) 220 °C, pH = 7; (**i**) 220 °C, pH = 13.

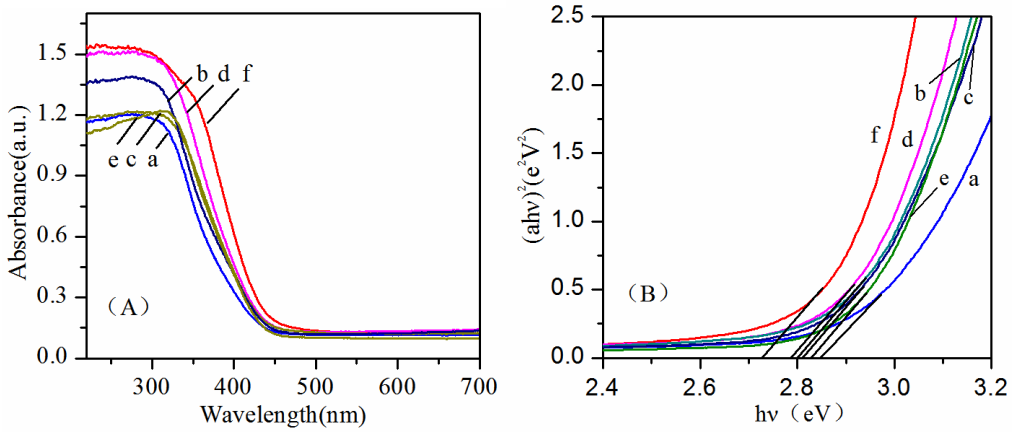

Figure 4. UV–Vis diffuse reflectance spectra (**A**) and plots of the $(ah\upsilon)^2$ (e^2V^2) versus $h\upsilon$ (eV) (**B**) of Bi_2WO_6 synthesized at different temperature and pH values. (a) 140 °C, pH = 1; (b) 140 °C, pH = 7; (c) 180 °C, pH = 1; (d) 180 °C, pH = 7; (e) 220 °C, pH = 1; (f) 220 °C, pH = 7.

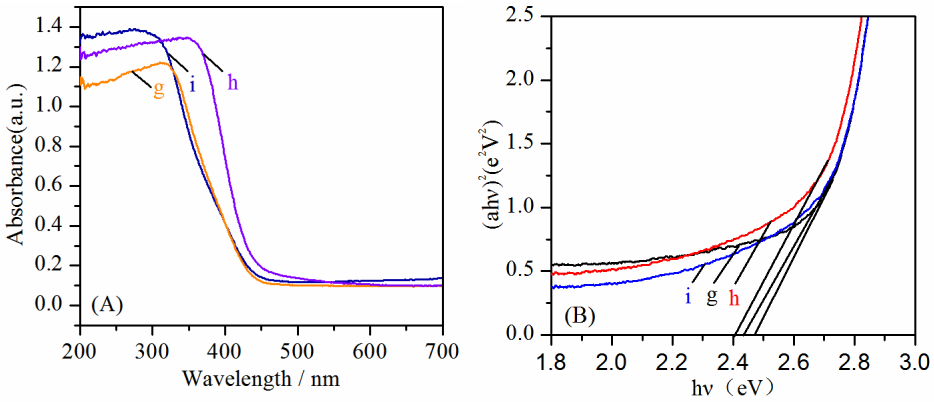

Figure 5. UV–Vis diffuse reflectance spectra (**A**) and plots of the $(ah\upsilon)^2$ (e^2V^2) versus hυ (eV) (**B**) of $Bi_{14}W_2O_{27}$ synthesized at different temperature and pH values. (g) 140 °C, pH = 13; (h) 180 °C, pH = 13; (i) 220 °C, pH = 13.

Table 2. The band gaps of Bi_2WO_6 and $Bi_{14}W_2O_{27}$.

	Sample	Hv (eV)
a	Bi_2WO_6-140 °C, pH = 1	2.85
b	Bi_2WO_6-140 °C, pH = 7	2.80
c	Bi_2WO_6-180 °C, pH = 1	2.81
d	Bi_2WO_6-180 °C, pH = 7	2.79
e	Bi_2WO_6-220 °C, pH = 1	2.83
f	Bi_2WO_6-220 °C, pH = 7	2.73
g	$Bi_{14}W_2O_{27}$-140 °C, pH = 13	2.47
h	$Bi_{14}W_2O_{27}$-180 °C, pH = 13	2.43
i	$Bi_{14}W_2O_{27}$-220 °C, pH = 13	2.41

The photocatalytic activities of the as-prepared catalysts under different temperature and pH values were comparatively evaluated by simultaneous degradation of MB under UV light irradiation. Figure 6A displays the degradation of MB within 60 min over different catalysts. It can be concluded that Bi_2WO_6 shows outstanding photocatalytic activities under UV light irradiation, while $Bi_{14}W_2O_{27}$ has almost no photocatalytic activities. In addition, Bi_2WO_6 catalysts synthesized by different pH values and temperatures show different catalytic performance. Clearly, after 60 min of reaction, the MB degradation efficiency approaches 91.6% (Figure 6h), higher than those achieved by using Figure 6g (84.5%), Figure 6e (83.3%), Figure 6d (77.3%), Figure 6b (72.5%), and Figure 6a (67.6%). In general, when Bi_2WO_6 is synthesized at the same temperature, pH = 7 shows better photocatalytic activities. When the catalyst is synthesized at the same pH, the higher synthetic temperature contributes to better catalytic activity.

The photocatalytic degradation of MB with Bi_2WO_6 as the catalyst follows first-order kinetic model. The relevant kinetics equation is shown as follows:

$$\ln \frac{C_t}{C} = kt,$$

where C is the added concentration of MB prior to reaction, C_t is the concentration of MB at different reaction time (t), k is an apparent rate constant, and t is the reaction time under UV irradiation condition. The kinetic plots for the MB degradation over Bi_2WO_6 catalyst were shown in Figure 6B, suggesting that the photocatalytic MB degradation reaction over Bi_2WO_6 catalyst is in accordance with the first-order kinetic reaction model. The achieved first-order kinetic constants (k) and corresponding coefficient (R^2) were summarized in Table 3. As seen in Table 3, the rate constants of the MB degradation over Bi_2WO_6 (220 °C, pH = 7, Table 3h) is higher than that over the rest of the Bi_2WO_6 samples (Table 3a,b,d,e,g). The activities of the synthesized samples are mainly related to the morphology and crystallinity. The

flower-like catalysts show an inferior catalytic activity, which is mainly ascribed to the fact that it is difficult for macromolecules MB to enter into the pores in flower-like catalysts [33].

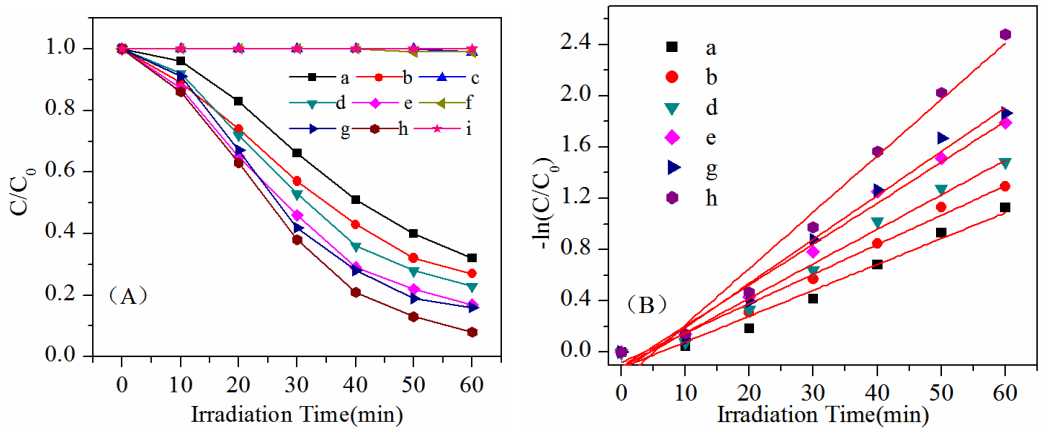

Figure 6. (**A**) Degradation of the MB over Bi_2WO_6 and $Bi_{14}W_2O_{27}$ synthesized under different temperature and pH values. (**B**) Plots of ln (C/C_0) versus irradiation time. (a) 140 °C, pH = 1; (b) 140 °C, pH = 7; (c) 140 °C, pH = 13; (d) 180 °C, pH = 1; (e) 180 °C, pH = 7; (f) 180 °C, pH = 13; (g) 220 °C, pH = 1; (h) 220 °C, pH = 7; (i) 220 °C, pH = 13.

Table 3. The first-order kinetic constants k (min^{-1}) and relative coefficient R^2 of Bi_2WO_6.

	Sample	K (min^{-1})	R^2
a	Bi_2WO_6-140 °C, pH = 1	0.020	0.966
b	Bi_2WO_6-140 °C, pH = 7	0.023	0.986
d	Bi_2WO_6-180 °C, pH = 1	0.032	0.984
e	Bi_2WO_6-180 °C, pH = 7	0.034	0.977
g	Bi_2WO_6-220 °C, pH = 1	0.035	0.980
h	Bi_2WO_6-220 °C, pH = 7	0.044	0.975

In order to further identify the reactive species during this reaction, we conducted the free radical capture experiments. Benzoquinone (BQ, 1 mM) as hydroxyl radical (•OH) scavenger, benzoquinone (BZQ 1 mM) as superoxide radical ($\bullet O_2^-$) scavenger, and disodium ethylenediamine tetraacetate (EDTA-Na_2 1mM) as hole (h^+) scavenger were added, respectively, in the above-mentioned reaction. It can be illustrated from Figure 7 that three radicals including •OH, h^+ and $\bullet O_2^-$ showed an improved photocatalytic performance, while the MB removal yield significantly decreased to 48.0%, from 91.6%, in the presence of IPA, suggesting that •OH should be the dominant photoreaction radical species, and the addition of EDTA-Na_2 and BZQ displays weaker effect on the MF degradation, which indicates that h^+ and $\bullet O_2^-$ contribute little to the degradation reaction.

In order to solve the serious wastewater pollution, Bi_2WO_6 which synthesized under 220 °C and the pH value of 7 were used to treat PPW, which were collected after secondary biochemical treatment, and the results are seen in Figure 8.

It can be clearly summarized that after 3 h of treatment, the COD_{Cr} and color degradation rate of PPW over Bi_2WO_6 under UV light (Bi_2WO_6/UV) were 75.1% and 87.3%, respectively. When H_2O_2 (10 mM) were added in the solution (Bi_2WO_6/UV/H_2O_2), the photo-Fenton-like reaction was produced, and the removals of COD_{Cr} and color of PPW were improved, 85.8% and 92.0% were degraded, respectively. The COD_{Cr} of treated PPW were 53.8 and 30.67 mg/L, satisfying the discharge standard of waste pollutants for the pulp and paper industry (GB3544-2008) in China.

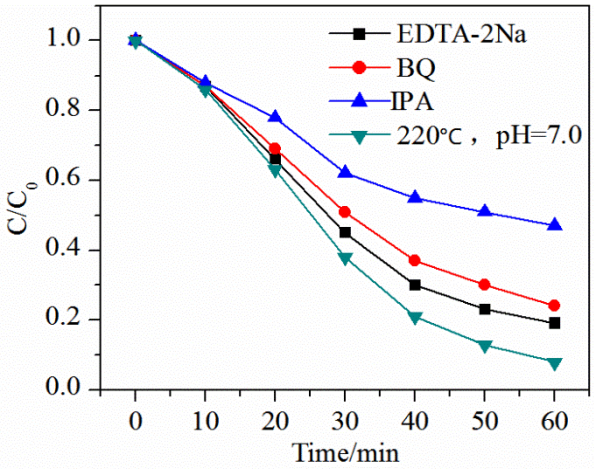

Figure 7. Effects of series scavengers on the MB degradation in the presence of Bi_2WO_6 synthesized under the temperature of 220 °C and pH value of 7.

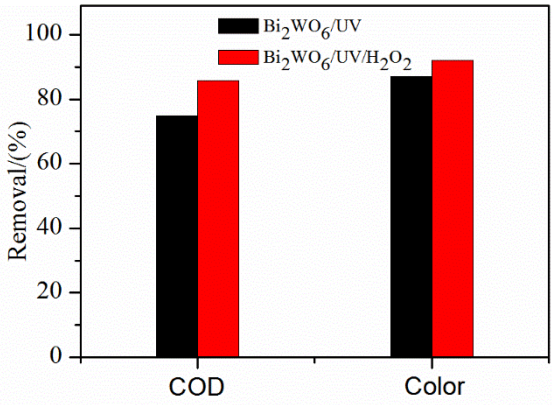

Figure 8. COD_{Cr} and color removal of PPW over Bi_2WO_6 and Bi_2WO_6/H_2O_2.

3. Experimental Section

3.1. Synthesis of the Samples

All chemicals were analytical grade and were used directly with no further purification. The Bi_2WO_6 nanoplates were prepared through one-step hydrothermal process [31]. The experimental procedures were as follows: First, 2.5 mmol of Na_2WO_4 was dissolved in 20 mL deionized water, 5.0 mmol of $Bi(NO_3)_3 \cdot 5H_2O$ was dissolved in 40 mL deionized water and was ultrasonic treated for 15 min to disperse evenly, then 20 mL of sodium tungstate solution was dropped into Bi $(NO_3)_3$ solution slowly under vigorous stirring. The pH value of the mixture solution was adjusted by adding 2.5 mol/L NaOH to 1, 7, and 13. After being stirred for 2 h, the suspension was then transferred into a 100 mL Teflon-lined autoclave and filled with deionized water up to 80%. The samples achieved from different pH values were placed under hydrothermal reaction for 12 h at 140, 180, and 220 °C, respectively. The resulting samples were collected and washed with deionized water and ethanol, and the obtained sample was then dried at 60 °C for 12 h.

3.2. Characterization

X-ray diffraction (XRD) spectra were carried out on a Rigaku Rotaflex diffractometer equipped with a rotating anode with Cu KR radiation with 2θ from 10° to 80°. Scanning electron microscopy (JSM-7001F, JEOL, Japan) was employed to clarify the morphologies of different samples. The surface

area of the samples were obtained by V-Sorb 2800. UV–Vis absorption spectra were carried out on a Shimadzu UV-2450 spectrometer.

3.3. Photocatalytic Tests

The photodegradation of MB were performed under UV irradiation condition with a 100 W mercury lamp in a cylindrical quartz reactor, with magnetic stirring apparatus and water circulation facility. Before illumination, the suspensions were vigorously stirred in the dark for 30 min to ensure the establishment of an adsorption equilibrium between the photocatalyst powder and MB. After that, the solution was exposed to UV light irradiation. For each experiment, 0.2 g catalyst was dispersed to 250 mL of MB solution (30 mg/L). After the reaction, 10 mL aliquots were collected every fifteen minutes and then centrifuged to separate the photocatalyst powders. The concentrations of MB were determined by analyzing the absorbance at 664 nm with a UV-2550 spectrophotometer (Shimadzu, Japan).

Poplar preconditioning refiner chemical alkaline peroxide mechanical pulp wastewater (PPW) was collected after biological treatment from a secondary sedimentation tank, and the characteristics of the wastewater are shown in Table 4. The wastewater was treated as the above process for 3 h with photodegradation. COD was measured according to Standard Methods (1998). The HACH-6000 spectrophotometer was used for the color measurements in the APHA Pt–Co (cobalt) unit.

Table 4. Characteristics of the PPW wastewater.

Sample	pH	COD_{Cr}/(mg/L)	Color/(Pt-Co)
PPW	7.16	216	745

4. Conclusions

The 3D flower-like microspheres and nanosheets Bi_2WO_6 photocatalyst was prepared by a facile hydrothermal approach. The pH value and temperature play an important role on the synthetic progress of Bi_2WO_6, resulting in differences in morphology, crystallinity, optical properties, and electronic properties. Photocatalytic tests show that Bi_2WO_6 synthesized under 220 °C and the pH of 7 has great photocatalytic activities. Furthermore, Bi_2WO_6 was also employed to treat the industrial PPW, which has a high removal of COD_{Cr} and color. Photo-Fenton-like reaction was produced with H_2O_2 addition and significantly increased the photocatalytic activities. From the results, it can be proposed that semiconductors may provide a promising platform for high-performance photocatalytic applications in industrial wastewater treatment.

Author Contributions: M.R. and X.Z. carried out the concepts, design, definition of intellectual content, literature search, data acquisition, data analysis and manuscript preparation, Q.T., L.L. and T.W. provided assistance for data interpretation, literature search and data analysis, A.P. and Y.D. carried out data analysis and manuscript editing, G.F. and L.D. performed project administration and funding acquisition.

Funding: This work was supported by the Jiangsu Key Laboratory for Biomass Energy and Material (JSBEM-S-201809), the National Key Research and Development Program of China (2017YFD0601005).

Conflicts of Interest: The authors declare no conflicts of interest.

References

1. Kamali, M.; Khodaparast, Z. Review on recent developments on pulp and paper mill wastewater treatment. *Ecotoxicol. Environ. Saf.* **2015**, *114*, 326–342. [CrossRef] [PubMed]
2. Machani, M.; Nourelfath, M.; D'Amours, S. A mathematically-based framework for evaluating the technical and economic potential of integrating bioenergy production within pulp and paper mills. *Biomass Bioenergy* **2014**, *63*, 126–139. [CrossRef]

3. Ashrafi, O.; Yerushalmi, L.; Haghighat, F. Application of dynamic models to estimate greenhouse gas emission by wastewater treatment plants of the pulp and paper industry. *Environ. Sci. Pollut. Res. Int.* **2013**, *20*, 1858–1869. [CrossRef] [PubMed]
4. Pokhrel, D.; Viraraghavan, T. Treatment of pulp and paper mill wastewater–a review. *Sci. Total Environ.* **2004**, *333*, 37–58. [CrossRef] [PubMed]
5. Ali, M.; Sreekrishnan, T.R. Aquatic toxicity from pulp and paper mill effluents a review. *Adv. Environ. Res.* **2001**, *5*, 175–196. [CrossRef]
6. Karrasch, B.; Parra, O.; Cid, H.; Mehrens, M.; Pacheco, P.; Urrutia, R.; Valdovinos, C.; Zaror, C. Effects of pulp and paper mill effluents on the microplankton and microbial self-purification capabilities of the Biobio River, Chile. *Sci. Total Environ.* **2006**, *359*, 194–208. [CrossRef]
7. Chandra, R.; Sharma, P.; Yadav, S.; Tripathi, S. Biodegradation of Endocrine-Disrupting Chemicals and Residual Organic Pollutants of Pulp and Paper Mill Effluent by Biostimulation. *Front. Microbiol.* **2018**, *9*, 960. [CrossRef]
8. Kamali, M.; Alavi-Borazjani, S.A.; Khodaparast, Z.; Khalaj, M.; Jahanshahi, A.; Costa, E.; Capela, I. Additive and additive-free treatment technologies for pulp and paper mill effluents: Advances, challenges and opportunities. *Water Resour. Ind.* **2019**, *21*. [CrossRef]
9. Ashrafi, O.; Yerushalmi, L.; Haghighat, F. Wastewater treatment in the pulp-and-paper industry: A review of treatment processes and the associated greenhouse gas emission. *J. Environ. Manag.* **2015**, *158*, 146–157. [CrossRef]
10. Izadi, A.; Hosseini, M.; Najafpour Darzi, G.; Nabi Bidhendi, G.; Pajoum Shariati, F. Treatment of paper-recycling wastewater by electrocoagulation using aluminum and iron electrodes. *J. Environ. Health Sci. Eng.* **2018**, *16*, 257–264. [CrossRef]
11. Sandberg, M.; Venkatesh, G.; Granström, K. Experimental study and analysis of the functional and life-cycle global warming effect of low-dose chemical pre-treatment of effluent from pulp and paper mills. *J. Clean. Prod.* **2018**, *174*, 701–709. [CrossRef]
12. Mansour, L.B.; Ksentini, I.; Elleuch, B. Treatment of wastewaters of paper industry by coagulation-electroflotation. *Desalination* **2007**, *208*, 34–41. [CrossRef]
13. Toczyłowska-Mamińska, R. Limits and perspectives of pulp and paper industry wastewater treatment—A review. *Renew. Sustain. Energy Rev.* **2017**, *78*, 764–772. [CrossRef]
14. Crini, G.; Lichtfouse, E. Advantages and disadvantages of techniques used for wastewater treatment. *Environ. Chem. Lett.* **2018**, *17*, 145–155. [CrossRef]
15. Kamali, M.; Gameiro, T.; Costa, M.E.V.; Capela, I. Anaerobic digestion of pulp and paper mill wastes—An overview of the developments and improvement opportunities. *Chem. Eng. J.* **2016**, *298*, 162–182. [CrossRef]
16. Savant, D.V.; Abdul-Rahman, R.; Ranade, D.R. Anaerobic degradation of adsorbable organic halides (AOX) from pulp and paper industry wastewater. *Bioresour. Technol.* **2006**, *97*, 1092–1104. [CrossRef]
17. Tambosi, J.L.; Di Domenico, M.; Schirmer, W.N.; José, H.J.; Moreira, F.P.M. Treatment of paper and pulp wastewater and removal of odorous compounds by a Fenton-like process at the pilot scale. *J. Chem. Technol. Biotechnol.* **2006**, *81*, 1426–1432. [CrossRef]
18. Catalkaya, E.C.; Kargi, F. Color, TOC and AOX removals from pulp mill effluent by advanced oxidation processes: A comparative study. *J. Hazard. Mater.* **2007**, *139*, 244–253. [CrossRef]
19. Ginni, G.; Adishkumar, S.; Rajesh Banu, J.; Yogalakshmi, N. Treatment of pulp and paper mill wastewater by solar photo-Fenton process. *Desalin. Water Treat.* **2013**, *52*, 2457–2464. [CrossRef]
20. Neoh, C.H.; Noor, Z.Z.; Mutamim, N.S.A.; Lim, C.K. Green technology in wastewater treatment technologies: Integration of membrane bioreactor with various wastewater treatment systems. *Chem. Eng. J.* **2016**, *283*, 582–594. [CrossRef]
21. Pirilä, M.; Saouabe, M.; Ojala, S.; Rathnayake, B.; Drault, F.; Valtanen, A.; Huuhtanen, M.; Brahmi, R.; Keiski, R.L. Photocatalytic Degradation of Organic Pollutants in Wastewater. *Top. Catal.* **2015**, *58*, 1085–1099. [CrossRef]
22. He, D.; Wang, L.; Xu, D.; Zhai, J.; Wang, D.; Xie, T. Investigation of photocatalytic activities over Bi(2)WO(6)/ZnWO(4) composite under UV light and its photoinduced charge transfer properties. *ACS Appl. Mater. Interfaces* **2011**, *3*, 3167–3171. [CrossRef] [PubMed]
23. Sun, S.; Wang, W.; Zhang, L.; Gao, E.; Jiang, D.; Sun, Y.; Xie, Y. Ultrathin {001}-oriented bismuth tungsten oxide nanosheets as highly efficient photocatalysts. *ChemSusChem* **2013**, *6*, 1873–1877. [CrossRef] [PubMed]

24. Tian, J.; Sang, Y.; Yu, G.; Jiang, H.; Mu, X.; Liu, H. A Bi_2WO_6-based hybrid photocatalyst with broad spectrum photocatalytic properties under UV, visible, and near-infrared irradiation. *Adv. Mater.* **2013**, *25*, 5075–5080. [CrossRef] [PubMed]
25. Gao, Y.; Shan, X.; Yang, W.; Chen, Y. Structure regulation and photocatalytic activity enhancement of Bi_2WO_6 by "double-effect modification" mode. *Int. J. Energy Res.* **2019**. [CrossRef]
26. Long, M.; Cai, W.; Kisch, H. Photoelectrochemical properties of nanocrystalline Aurivillius phase Bi_2MoO_6 film under visible light irradiation. *Chem. Phys. Lett.* **2008**, *461*, 102–105. [CrossRef]
27. Liang, Y.; Shi, J.; Fang, B. Synthesis and electrochemical performance of bismuth tungsten oxides with different composition and morphology. *Chem. Phys. Lett.* **2019**, *716*, 112–118. [CrossRef]
28. Yao, S.; Wei, J.; Huang, B.; Feng, S.; Zhang, X.; Qin, X.; Wang, P.; Wang, Z.; Zhang, Q.; Jing, X.; et al. Morphology modulated growth of bismuth tungsten oxide nanocrystals. *J. Solid State Chem.* **2009**, *182*, 236–239. [CrossRef]
29. Zhang, L.; Wang, W.; Zhou, L.; Xu, H. Bi_2WO_6 nano- and microstructures: Shape control and associated visible-light-driven photocatalytic activities. *Small* **2007**, *3*, 1618–1625. [CrossRef]
30. Shang, Y.; Cui, Y.; Shi, R.; Yang, P. Effect of acetic acid on morphology of Bi_2WO_6 with enhanced photocatalytic activity. *Mater. Sci. Semicond. Process.* **2019**, *89*, 240–249. [CrossRef]
31. Hojamberdiev, M.; Katsumata, K.-I.; Morita, K.; Bilmes, S.A.; Matsushita, N.; Okada, K. One-step hydrothermal synthesis and photocatalytic performance of $ZnWO_4/Bi_2WO_6$ composite photocatalysts for efficient degradation of acetaldehyde under UV light irradiation. *Appl. Catal. A: Gen.* **2013**, *457*, 12–20. [CrossRef]
32. Wang, J.-J.; Tang, L.; Zeng, G.-M.; Zhou, Y.-Y.; Deng, Y.-C.; Fan, C.-Z.; Gong, J.-L.; Liu, Y.-N. Effect of bismuth tungstate with different hierarchical architectures on photocatalytic degradation of norfloxacin under visible light. *Trans. Nonferrous Met. Soc. China* **2017**, *27*, 1794–1803. [CrossRef]
33. Tian, Q.-W.; Li, N.-X.; Liu, J.-H.; Wang, M.; Deng, J.-Q.; Zhou, J.-C.; Ma, Q.-H. Catalytic Hydrogenation of Alkali Lignin to Bio-oil Using Fullerene-like Vanadium Sulfide. *Energy Fuels* **2014**, *29*, 255–261. [CrossRef]